Elastohydrodynamic relaxation of soft and deformable microchannels

Gabriel Guyard, Frédéric Restagno, Joshua D Mcgraw

To cite this version:

Gabriel Guyard, Frédéric Restagno, Joshua D Mcgraw. Elastohydrodynamic relaxation of soft and deformable microchannels. Physical Review Letters, 2022, 129 (20), 10.1103/PhysRevLett.129.204501 . hal-03719718v2

HAL Id: hal-03719718
https://hal.science/hal-03719718v2

Submitted on 4 Nov 2022

Elastohydrodynamic relaxation of soft and deformable microchannels

Gabriel Guyard,[1, 2, 3] Frédéric Restagno,[3] and Joshua D. McGraw[1, 2, *]
[1] *Gulliver CNRS UMR 7083, PSL Research University,*
ESPCI Paris, 10 rue Vauquelin, 75005 Paris, France
[2] *IPGG, 6 rue Jean-Calvin, 75005 Paris, France*
[3] *Université Paris-Saclay, CNRS, Laboratoire de Physique des Solides, 91405, Orsay, France*
(Dated: November 4, 2022)

Hydrodynamic flows in compliant channels are of great interest in physiology and microfluidics. In these situations, elastohydrodynamic coupling leads to: (i) a nonlinear pressure-*vs.*-flow-rate relation, strongly affecting the hydraulic resistance; and (ii), because of the compliance-enabled volume storage, a finite relaxation time under a step-wise change in pressure. This latter effect remains relatively unexplored, even while the time scale can vary over a decade in typical situations. In this study we provide time-resolved measurements of the relaxation dynamics for thin and soft, rectangular microfluidic channels. We describe our data using a perturbative lubrication approximation of the Stokes equation coupled to linear elasticity, while taking into account the effect compliance and resistance of the entrance. The modeling allows to completely describe all of the experimental results. Our work is relevant for any microfluidic scenario wherein a time-dependent driving is applied and provides a first step in the dynamical description of compliant channel networks.

To force the movement of fluid through a channel, a pressure drop must be applied across its ends. If the bounding walls of this simple flow domain are compliant, a pressure-induced deformation can strongly affect the flow as compared to the non-compliant case. This elastohydrodynamic coupling is often encountered, and the pipe-flow case is referred to as soft hydraulics [1]. Particularly, the flow modification can give a non-linear pressure-*vs.*-flow-rate relation [2, 3], with the flow resistance changing by an order of magnitude or more. Upon a pressure change, however, the relaxation to a new deformation profile is not instantaneous. The pipe thus settles into a new configuration over a little-investigated, pressure-dependent time scale at the focus of this Letter.

Elastohydrodynamics (EHD) was historically studied in the context of lubrication of rough, solid contacts [4–6], often for heavy mechanical applications and remains a key ingredient in modern tribology [7]. Conversely, the lubrication of soft materials has attracted increasing attention in the last decades [8–12] due in part to its relevance in biology and microtechnologies. Examples include joint lubrication [13], eyelid wiper mechanics [14], and the deformation of blood vessels under flow-induced pressure [15–19]. At microscales, EHD interactions may affect the transport of blood cells [20] because of the emergent lift forces arising from the fluid-mediated soft-substrate deformation [21].

Concerning soft technologies, microfluidics is of significant interest [22]. Indeed, microchannels are typically made with soft elastomers —*e.g.* polydimethylsiloxane (PDMS)— allowing for fast prototyping, design fidelity, and transparency [23, 24]. Compliance is a key attribute for applications such as organ-on-a-chip [25, 26] or wearable technologies [27, 28]. Targeted actuation of deformable pipes also allows to generate and manipulate flows at the scale of a single channel [29–31], or in complex networks [32] as in the plant kingdom [33]. Finally, soft components can be used as pressure-controlled valves serving as building blocks for the logic gate components in state-of-the-art microdevices [34–36].

While many soft-hydraulics studies focus on the steady state, compliance is also expected to have dynamic effects. This deformability leads to volume storage capacity [37], schematically indicated in Fig. 1(a), which in addition to changing the resistance of a narrow channel, implies a characteristic response time of the system by analogy with electronics [38, 39], see Fig. 1(b). This dynamic response was used for example to attenuate parasitic fluctuations in syringe-pump driven flows [40], and limits the production rate in stop-flow lithography [41].

With dynamical aspects of soft hydraulics already finding applications, it is imperative to characterize the temporal response of compliant microchannels. Here we experimentally and theoretically investigate the response of thin, soft microfluidic channels to step-wise pressure perturbations. We use an EHD model in the lubrication limit applied to such devices. As previously [2, 3, 42], this approach allows to rationalise the nonlinear relation between pressure and flow rate. Performing a perturbation analysis and, crucially, specifying the capacitance and resistance of the peripheral components, the pressure-dependent relaxation dynamics of the entire experimental system is revealed. Our approach includes an asymptotic analysis of the general high- and low-pressure limits, along with the full crossover requiring complete specification of the microsystem.

The microfluidic chips used here consisted of rectangular channels with length $L = 4.0$ cm between the inlet/outlet centers of radius $d_\mathrm{c} = 1.0$ mm (*cf.* the Supplemental Material, SM §S.I at Ref. [43], for a full list of symbols). The channel widths were $w = \{200, 500, 1000, 2000\}$ µm, with uncertainty of order a

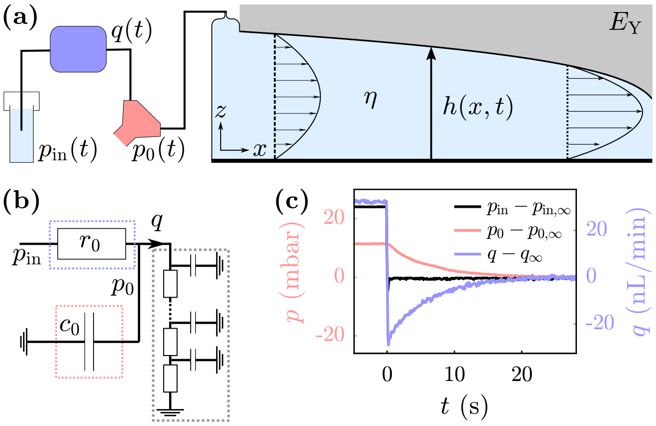

Figure 1. **(a)** Schematics of the microfluidic setup, including a flow sensor, a pressure sensor and a soft channel. **(b)** Equivalent electronic circuit, the flow sensor modeled as an ideal resistance r_0, the pressure sensor as a capacitance c_0, and the soft channel as a series of infinitesimal resistances and capacities as in a transmission line. **(c)** Shifted, imposed p_{in} and measured p_0 and q as a function of t, with long-time values of $p_{\mathrm{in},\infty} = 1301$ mbar, $p_{0,\infty} = 862$ mbar and $q_\infty = 1058$ nL/ min.

few micrometers, and undeformed heights $h_0 = 5.0 \pm 0.1$ µm. The molds were characterized with a mechanical profilometer (Bruker Dektak). Liquid reservoirs were connected to chips using tubing with negligible hydraulic resistance and compliance (PEEK, IDEX 1581, ID 0.25 mm, OD 1/32", length *ca.* 50 cm). Microchannels were fabricated [44] from PDMS (Momentive RT 615 A & B) including 10 wt.% cross-linker, and cured at 170 °C for 15 minutes.

Flow and pressure sensors (Elveflow MFS1 and MPS2) provided time-resolved measurements of the flow rate q and pressure p_0, relative to atmospheric pressure, at the chip inlet. Ultra-pure water (Milli-Q, 18.2 MΩ cm, viscosity $\eta = 1.00 \pm 0.02$ mPa s) at room temperature was driven using a pressure controller (Elveflow OB1 mk3+), with constant pressure, p_{in}, imposed across the input sensors and the microchannel, see Fig. 1(a). After reaching steady state, p_{in} was suddenly dropped and the temporal responses $q(t)$ and $p_0(t)$ recorded until a new steady state was reached; a selection of raw data is also shown in the SM §S.II.

Figure 1(c) shows a set of recorded signals for $p_{\mathrm{in}}(t)$, $p_0(t)$, and $q(t)$ after a pressure drop. Each signal is shifted to its long-time, steady value, denoted $p_{\mathrm{in},\infty}$, $p_{0,\infty}$, and q_∞, respectively. While p_{in} varied on a time scale of just 0.1 s, p_0 and q reach new steady states after a much longer transient time, τ_{t}, of order 10 s, depending on the initial input pressure and channel geometry. In the following we study the dependence of q_∞ and τ_{t}, on $p_{0,\infty}$ and w.

In Fig. 2 is shown the scaled relation between the dimensionless, steady-state flow rate Q_∞ and pressure $P_{0,\infty}$ for all of the chip geometries used here. While the raw data is shown in SM §S.III, here the pressure is normalized by the natural scale $p^* = E^* h_0/w$. The semi-infinite slab case [2, 45] gives $E^* \approx E_{\mathrm{Y}}/0.5427(1-\nu^2)$, where ν and E_{Y} are the Poisson ratio and Young's modulus of the material [46]. The flow rate is normalized by p^*/r_{c}, with $r_{\mathrm{c}} = 12\eta L/w h_0^3$ the hydraulic resistance of an undeformed rectangular channel [47]. Such a normalization gives a single master curve after adjusting the data to the fitting parameters for each chip, p^* and r_{c}. These latter follow the expected scaling with w, as seen in the insets, the top one with no fitting parameter on the line. The slope of the line of the bottom inset finally gives a measurement of $E_{\mathrm{Y}} = 1.07 \pm 0.03$ MPa, consistent with the typical value for this PDMS [48]. In contrast to rigid pipe flow [47, 49], the flow-rate response of these channels is highly nonlinear. Indeed, when the pressure is increased, the channel's resistance decreases due to its dilation.

Considering the dynamics, in Fig. 3 is shown $p_0 - p_{0,\infty}$ as a function of time in a 200 µm-wide channel for several $p_{0,\infty}$; straight lines in semi-log axis indicate exponential relaxations, allowing a precise determination of τ_{t}. The inset of Fig. 3 thus shows the characteristic time τ_{t} as a function of $p_{0,\infty}$, the relaxation time decreasing by a factor of 5 across the accessed range of $p_{0,\infty}$. As deformation allows the channel to store a pressure-dependent fluid volume, a microfluidic chips is a liquid-storage capacitor. Furthermore, the channels exhibit resistance, so that they are RC fluidic circuits [38, 47]. To rationalize the non-linearity of q_∞ with $p_{0,\infty}$, as well as the dependence of τ_{t} on $p_{0,\infty}$, we propose the following elastohydrodynamic model.

Considering the one dimensional limit since $h_0 \ll w \ll L$, we denote $h(x,t)$ the time-dependent height of the microchannel along the center line and along the flow direc-

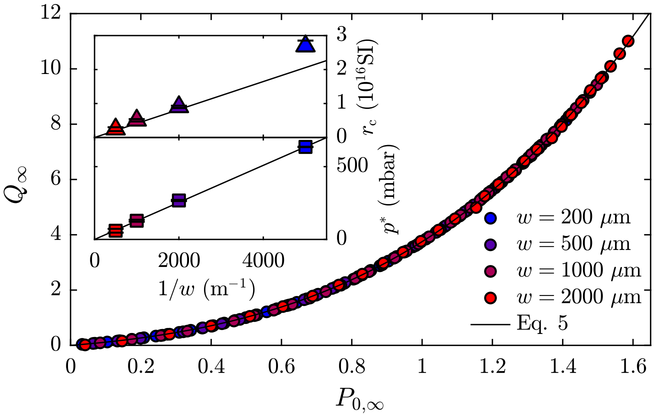

Figure 2. Dimensionless steady-state flow rate $Q_\infty = q_\infty r_{\mathrm{c}}/p^*$ as a function of the dimensionless steady-state inlet pressure $P_{0,\infty} = p_{0,\infty}/p^*$ for channels of the indicated widths. The solid line indicates the model of Eq. 5. Error bars are smaller than symbol size; insets show fitting parameters p^* and r_{c}.

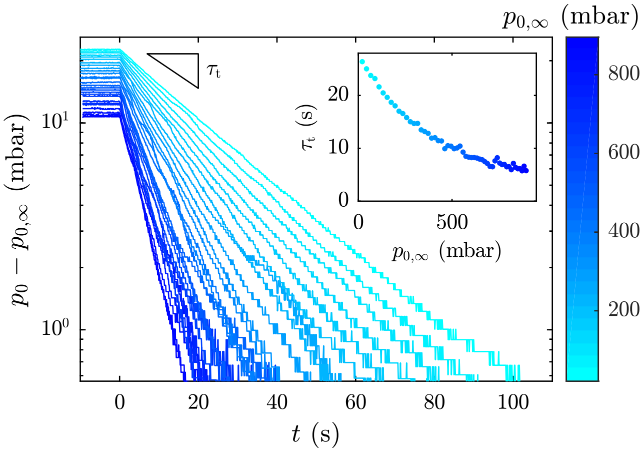

Figure 3. Inlet pressure $p_0 - p_{0,\infty}$ as a function of time t in a 200 µm-wide channel, the color bar indicating $p_{0,\infty}$. The inset shows the exponential relaxation time, obtained from best fits, as a function of $p_{0,\infty}$. Error bars are smaller than symbol size.

tion, x, and $p(x,t)$ the pressure field within the channel. In the lubrication limit, the Reynolds equation [50] expresses conservation of volume for incompressible, Newtonian fluids:

$$\partial_t h = \frac{1}{12\eta} \partial_x \left(h^3 \partial_x p \right) . \tag{1}$$

Since the former equation introduces the unknown fields $h(x,t)$ and $p(x,t)$, an elastic model is needed to connect the height profile to the pressure field. Even though the height profile varies in both the streamwise x and transverse y directions, as detailed by Christov and coworkers [3, 42], we consider a local, linear elastic response of the surrounding material along the center line:

$$h(x,t) = h_0 + \frac{w}{E^*} p(x,t) \ , \tag{2}$$

neglecting possible viscous losses in the PDMS [51].

To close the problem, we consider the boundary conditions. At the outlet we simply have $p(L,t) = 0$. At the inlet, we account for the peripheral sensors. Using the classic analogy between microfluidics and electronics [38, 39, 47], the setup is akin to the circuit depicted in Fig. 1(b). The flow sensor, composed of a thin hard glass capillary, is modeled as an ideal resistance r_0. The pressure sensor, including deformable parts, is modeled with a negligibly-resistant capacity $c_0 = \mathrm{d}\Omega/\mathrm{d}p_0$ where Ω is the volume of fluid stored in the sensor with pressure playing the role of the electric potential. Flux conservation then reads as the electrical current flowing through a resistance and the discharge current of a capacitor on one side, and the current at the entrance of a non-linear transmission line (*cf.* Ref. [52]) on the other:

$$\frac{p_\mathrm{in} - p_0}{r_0} - c_0 \frac{\mathrm{d}p_0}{\mathrm{d}t} = \left(- \frac{w h^3}{12\eta} \partial_x p \right) \bigg|_{x=0} . \tag{3}$$

Non-dimensionalizing, we take: $h = h_0 H$, $x = LX$, $t = \tau_\mathrm{c} T$ with $\tau_\mathrm{c} = 12\eta w L^2 / h_0^3 E^*$ as in Ref. [41], and pressures take the form $p = p^* P$. Combining Eq. 1 and Eq. 2, we obtain the elastohydrodynamic equation for the pressure field within the chip:

$$\partial_T P = \partial_X \left[(1+P)^3 \, \partial_X P \right] . \tag{4}$$

In the steady state, with a constant inlet pressure $P_{0,\infty}$ and null outlet pressure, a single integration of Eq. 4 gives $P_\infty(X) = \left[(1-X)((1+P_{0,\infty})^4 - 1) + 1 \right]^{1/4} - 1$. From this pressure profile, we compute the steady flux Q_∞ using the square-bracketed term of Eq. 4:

$$Q_\infty = \frac{1}{4} \left[(1+P_{0,\infty})^4 - 1 \right] = \frac{1}{4} \Pi \ , \tag{5}$$

having introduced $\Pi = (1+P_{0,\infty})^4 - 1$. Equation 5 has a similar form to the expressions given previously [3, 42], and we note the excellent agreement between this model (black line) and the data of Fig. 2.

Addressing the time-dependent problem now, we linearize Eq. 4, introducing $\delta P(X,T) = P(X,T) - P_\infty(X)$. At $\mathcal{O}(\delta P^1)$ and after the linear change of variables $\tilde{X} = (1-X)\Pi + 1$ and $\tilde{T} = \Pi^2 T$, we obtain:

$$\partial_{\tilde{T}} \delta P = \partial^2_{\tilde{X}} \left[\tilde{X}^{3/4} \delta P \right] . \tag{6}$$

Looking for separable solutions of Eq. 6, we propose $\delta P(\tilde{X}, \tilde{T}) = A(\tilde{X}) B(\tilde{T})$. Using the boundary condition for $\delta P = 0$ at $\tilde{X} = 1$, we obtain $B_\lambda(\tilde{T}) = \exp(-\lambda \tilde{T})$, confirming the experimentally observed exponential pressure decay; determining the eigenvalues λ remains. For the spatial part, we have [53] $A_\lambda(\tilde{X}) = \alpha_\lambda \tilde{X}^{-1/4} \mathcal{C}_{\frac{4}{5}} \left(\frac{8\sqrt{\lambda}}{5} \tilde{X}^{5/8} \right)$, where α_λ is an integration constant. The function $\mathcal{C}_\nu$ is a linear combination of Bessel functions, here of the form $\mathcal{C}_\nu(x) = \mathrm{Y}_{\frac{4}{5}} \left(\frac{8\sqrt{\lambda}}{5} \right) \mathrm{J}_\nu(x) - \mathrm{J}_{\frac{4}{5}} \left(\frac{8\sqrt{\lambda}}{5} \right) \mathrm{Y}_\nu(x)$, satisfying $p(L,t) = 0$.

For the boundary condition at the channel entrance, the full solution $P_\infty(X) + \delta P(\tilde{X}, \tilde{T})$ can be injected into the dimensionless version of Eq. 3. Such a substitution gives a constraining equation on the eigenvalues, λ, after evaluation at $\tilde{X}_0 = 1 + \Pi$, *i.e.* the channel entrance:

$$\frac{1}{\mathcal{R} \tilde{X}_0^{3/8}} \left(\mathcal{T} \sqrt{\lambda} \Pi - \frac{1}{\sqrt{\lambda} \Pi} \right) = \frac{\mathcal{C}_{-\frac{1}{5}} \left(\frac{8\sqrt{\lambda}}{5} \tilde{X}_0^{5/8} \right)}{\mathcal{C}_{\frac{4}{5}} \left(\frac{8\sqrt{\lambda}}{5} \tilde{X}_0^{5/8} \right)} \ , \tag{7}$$

with $\mathcal{R} = r_0 / r_\mathrm{c}$ and $\mathcal{T} = \tau_0 / \tau_\mathrm{c}$ where $\tau_0 = r_0 c_0$ is the inlet time scale. Recalling that the experimentally measured pressure relaxations of Fig. 3 are well described by simple exponential decays, and denoting λ_s smallest eigenvalue satisfying Eq. 7, the experimentally measured time scale is then assumed to be

$$\frac{\tau_\mathrm{t}}{\tau_\mathrm{c}} = \frac{1}{\Pi^2} \lambda_\mathrm{s}^{-1}(\Pi, \mathcal{R}, \mathcal{T}) \ , \tag{8}$$

in accordance with the definition of $\tilde{T}$. This relation shows that the relaxation time scale is a function of the pressure through Π, and in particular depends on the details of the input resistance and capacitance, here reflected through the dimensionless $\mathcal{R}$ and $\mathcal{T}$.

We are not aware of analytic solutions for Eq. 7; nevertheless, the asymptotic behavior can be assessed. At low pressure, there is no significant channel deformation ($p_0 \ll p^*$) such that the chip is an ideal resistance. We do not expect the relaxation time to be pressure dependent in this limit. Conversely at high pressure, the deformation makes the resistance of the chip pressure dependent. According to Eq. 5, we have a chip resistance, and thus a timescale proportional to $P_{0,\infty}^{-3}$. We thus look for asymptotic, power-law solutions to Eq. 7, $\lambda_\mathrm{s} \approx \beta^2 \Pi^\gamma$, with constant β and γ. Using asymptotic developments of the Bessel functions (SM, §S.IV), we confirm the power laws:

$$\frac{\tau_\mathrm{t}}{\tau_\mathrm{c}} = \frac{1}{\beta^2} \quad : \quad \Pi \ll 1 \,, \tag{9}$$

$$\frac{\tau_\mathrm{t}}{\tau_\mathrm{c}} = \frac{1}{\beta^2 P_{0,\infty}^3} \quad : \quad \Pi \gg 1 \,. \tag{10}$$

Here, β satisfies $\mathcal{T}\beta^2 - \mathcal{R}\beta\cot(\beta) - 1 = 0$ and $\mathcal{T}\beta/\mathcal{R} = \mathrm{J}_{-\frac{1}{5}}\left(8\beta/5\right)/\mathrm{J}_{\frac{4}{5}}\left(8\beta/5\right)$ in the low- and high-Π limits; we also note that $\mathcal{T}$ and $\mathcal{R}$ may differ in these limits.

For intermediate pressures, Eq. 8 is solved numerically for prescribed values of $\{\Pi, \mathcal{R}, \mathcal{T}\}$, thus necessitating characterizations of the input r_0 and c_0. The former was determined by measuring $p_{\mathrm{in},\infty}$ versus q_∞ in the presence of the flow meter only. The data (SM §S.V) are well described by a straight line, giving $r_0 = 2.50 \pm 0.01$ kPa s/nL, consistent with a rigid glass capillary of diameter 25 µm and length 2.4 cm filled with water of viscosity $\eta = 1.0$ mPa s [47]. The value of c_0 is assessed by plugging the circuit at the pressure sensor outlet and removing the microchannel, assuming that the resulting relaxation time satisfies $\tau_0 = r_0 c_0$. The inset of Fig. 4 shows τ_0 as a function of $p_{0,\infty}$ for such a plugged experiment, indicating a clearly nonlinear inlet capacity.

Assuming that the non-trivial capacity at the channel inlet is dominated by trapped air, we use the ideal gas law to estimate $c_0 = c_1(1 + p_{0,\infty}/p_\mathrm{atm})^{-2} + c_2$. Here p_atm=101 kPa is the atmospheric pressure, $c_1 = \Omega_\mathrm{a}/p_\mathrm{atm}$, with Ω_a the trapped air volume at atmospheric pressure. The second term, c_2, describes any other linear capacity, is assumed to be connected to the atmosphere and is thus in parallel with c_1. The solid line in the inset provides an excellent fit using this ideal-gas-like inlet capacity, with $c_1 = 20.9 \pm 0.1$ nL kPa^{-1} and $c_2 = 0.2 \pm 0.1$ nL kPa^{-1} $\ll c_1$. The value of c_1 corresponds to a resting gas volume of 2.1 µL, which compares reasonably to the internal volume of the pressure sensor of 7.5 µL as provided by the manufacturer.

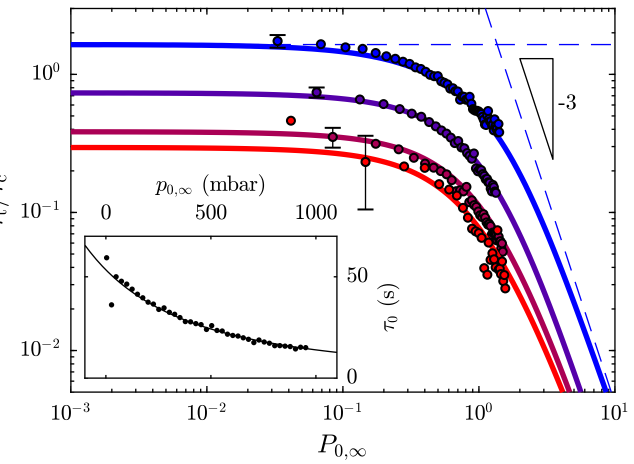

Figure 4. $\tau_\mathrm{t}/\tau_\mathrm{c}$ as a function of $P_{0,\infty}$ for four channels of different widths, color map as in Fig. 2. Single, typical error bars are shown for each data set. Solid lines represent numerical solutions of the model of Eq. 8 using ideal input resistance and an ideal-gas-like input capacitance, with dashed lines the asymptotic developments (Eqs. 9 and 10), for the 200 µm-wide channel. Inset: τ_0 as a function of $p_{0,\infty}$ for the plugged experiment. Error bars are smaller than symbol size. The solid line is a fit to the model including an ideal gas capacitance.

Making a full test of the model for our complete microfluidic system, Figure 4 shows the normalized relaxation time $\tau_\mathrm{t}/\tau_\mathrm{c}$ as a function of $P_{0,\infty}$ for all channel widths used here. The solid lines represent the numerical solution of the problem (Eqs. 7 and 8), where Eq. 7 is solved numerically using the aforementioned ideal resistance value and the ideal-gas, pressure-dependent capacitance. For this data the best-fitting values were $c_1 = 8.6 \pm 0.4$ nL kPa^{-1} and $c_2 = 2.1 \pm 0.2$ nL kPa^{-1}, respectively. Here the larger value of c_2 corresponds well to the linear capacity of the circular channel inlet, approximated by $c_2 \approx d_\mathrm{c}^3/E^* \approx 1$ nL kPa^{-1}. The smaller value of c_1 suggests that less air was trapped compared to the calibration. We additionally show the asymptotic behaviors, where the equations for prefactors β were solved graphically using the limiting values of $\mathcal{T}$ and $\mathcal{R}$. Our model describes the data well over more than one decade of normalized pressures and four chip geometries, all fitted using the same c_1 and c_2, the experiments having been performed sequentially.

In conclusion, we have used time-resolved pressure and flow-rate measurements to characterize the relaxation dynamics of compliant microfluidic channels. We recover the well-known, quartic pressure-*vs.*-flow-rate relation for straight, rectangular channels. Additionally, we measured a full series of pressure-dependent relaxation time scales resulting from step-wise pressure perturbations in a series of chip widths. Our main results are: (*i*) the chip inlet impedance cannot be neglected; and (*ii*), there is a strong pressure dependence on the relaxation time scale that cannot be simply predicted by dimensional analysis. A perturbation analysis of the lubrication-approximated microflow problem, coupled to a linear elasticity of the channel walls and considering the inlet impedance, accounts fully for the measured time scales. In a more general context, ours is a simple unit of any potential compliant flow network. Our analysis could thus be exploited in a broad range of micro-biological, and micro-technological contexts already finding applications.

The authors thank Ivan C. Christov, Thomas Salez, Stéphane Jouenne and Andreas Carlson for fruitful discussions. The authors benefited from the financial support of the Agence Nationale de la Recherche (ANR) under the CoPinS (ANR-19CE06-0021) grant, and of the Institut Pierre-Gilles de Gennes (Equipex ANR-10-EQPX-34 and Labex ANR-10-LABX-31), PSL Research University (Idex ANR-10-IDEX-0001-02). Total Energies is also gratefully acknowledged for financial support under contract TOTAL DS3700 – CNRS 2019200804.

---

[*] joshua.mcgraw@cnrs.fr

[1] I. C. Christov, Journal of Physics: Condensed Matter **34**, 063001 (2021).
[2] T. Gervais, J. El-Ali, A. Günther, and K. F. Jensen, Lab on a Chip **6**, 500 (2006).
[3] I. C. Christov, V. Cognet, T. C. Shidhore, and H. A. Stone, Journal of Fluid Mechanics **841**, 267 (2018).
[4] R. Stribeck, *Kugellager für beliebige Belastungen* (Springer, 1901).
[5] R. Gohar and A. Cameron, Nature **200**, 458 (1963).
[6] K. Johnson, J. Greenwood, and S. Poon, Wear **19**, 91 (1972).
[7] J. Hansen, M. Björling, and R. Larsson, Scientific Reports **10**, 22250 (2020).
[8] S. Leroy and E. Charlaix, Journal of Fluid Mechanics **674**, 389 (2011).
[9] Y. Wang, C. Dhong, and J. Frechette, Physical review letters **115**, 248302 (2015).
[10] B. Saintyves, T. Jules, T. Salez, and L. Mahadevan, Proceedings of the National Academy of Sciences **113**, 5847 (2016).
[11] Z. Zhang, V. Bertin, M. Arshad, E. Raphaël, T. Salez, and A. Maali, Phys. Rev. Lett. **124**, 054502 (2020).
[12] V. Bertin, Y. Amarouchene, E. Raphaël, and T. Salez, Journal of Fluid Mechanics **933**, A23 (2022).
[13] S. Jahn, J. Seror, and J. Klein, Annual Review of Biomedical Engineering **18**, 235 (2016).
[14] M. Jones, G. Fulford, C. Please, D. McElwain, and M. J. Collins, Bulletin of Mathematical Biology **70**, 323 (2008).
[15] K. Perktold and G. Rappitsch, Journal of biomechanics **28**, 845 (1995).
[16] C. A. Figueroa, I. E. Vignon-Clementel, K. E. Jansen, T. J. Hughes, and C. A. Taylor, Computer methods in applied mechanics and engineering **195**, 5685 (2006).
[17] M. Heil and A. L. Hazel, Annual review of fluid mechanics **43**, 141 (2011).
[18] M. Hirschhorn, V. Tchantchaleishvili, R. Stevens, J. Rossano, and A. Throckmorton, Medical engineering & physics **78**, 1 (2020).
[19] C. A. Taylor, T. J. Hughes, and C. K. Zarins, Annals of biomedical engineering **26**, 975 (1998).
[20] H. S. Davies, D. Débarre, N. El Amri, C. Verdier, R. P. Richter, and L. Bureau, Physical review letters **120**, 198001 (2018).
[21] J. M. Skotheim and L. Mahadevan, Phys. Rev. Lett. **92**, 245509 (2004).
[22] H. Xia, J. Wu, J. Zheng, J. Zhang, and Z. Wang, Lab on a Chip **21**, 1241 (2021).
[23] Y. Xia and G. M. Whitesides, Annual Review of Materials Science **28**, 153 (1998).
[24] K. Raj M and S. Chakraborty, Journal of Applied Polymer Science **137**, 48958 (2020).
[25] D. Huh, B. D. Matthews, A. Mammoto, M. Montoya-Zavala, H. Y. Hsin, and D. E. Ingber, Science **328**, 1662 (2010).
[26] J. U. Lind, T. A. Busbee, A. D. Valentine, F. S. Pasqualini, H. Yuan, M. Yadid, S.-J. Park, A. Kotikian, A. P. Nesmith, P. H. Campbell, *et al.*, Nature materials **16**, 303 (2017).
[27] S. Xu, Y. Zhang, L. Jia, K. E. Mathewson, K.-I. Jang, J. Kim, H. Fu, X. Huang, P. Chava, R. Wang, *et al.*, Science **344**, 70 (2014).
[28] J. C. Yeo, C. T. Lim, *et al.*, Lab on a Chip **16**, 4082 (2016).
[29] D. P. Holmes, B. Tavakol, G. Froehlicher, and H. A. Stone, Soft Matter **9**, 7049 (2013).
[30] F. J. Meigel, P. Cha, M. P. Brenner, and K. Alim, Physical Review Letters **123**, 228103 (2019).
[31] E. Virot, V. Spandan, L. Niu, W. M. Van Rees, and L. Mahadevan, Physical Review Letters **125**, 058102 (2020).
[32] J. W. Rocks, A. J. Liu, and E. Katifori, Physical Review Letters **126**, 028102 (2021).
[33] K. Park, A. Tixier, M. Paludan, E. Østergaard, M. Zwieniecki, and K. H. Jensen, Phys. Rev. Fluids **6**, 123102 (2021).
[34] B. Mosadegh, C.-H. Kuo, Y.-C. Tung, Y.-s. Torisawa, T. Bersano-Begey, H. Tavana, and S. Takayama, Nature physics **6**, 433 (2010).
[35] J. A. Weaver, J. Melin, D. Stark, S. R. Quake, and M. A. Horowitz, Nature Physics **6**, 218 (2010).
[36] P. N. Duncan, T. V. Nguyen, and E. E. Hui, Proceedings of the National Academy of Sciences **110**, 18104 (2013).
[37] D. C. Leslie, C. J. Easley, E. Seker, J. M. Karlinsey, M. Utz, M. R. Begley, and J. P. Landers, Nature Physics **5**, 231 (2009).
[38] K. W. Oh, K. Lee, B. Ahn, and E. P. Furlani, Lab on a Chip **12**, 515 (2012).
[39] D. J. Preston, P. Rothemund, H. J. Jiang, M. P. Nemitz, J. Rawson, Z. Suo, and G. M. Whitesides, Proceedings of the National Academy of Sciences **116**, 7750 (2019).
[40] Z. Jiao, J. Zhao, Z. Chao, Z. You, and J. Zhao, Microfluidics and Nanofluidics **23**, 1 (2019).
[41] D. Dendukuri, S. S. Gu, D. C. Pregibon, T. A. Hatton, and P. S. Doyle, Lab Chip **7**, 818 (2007).
[42] X. Wang and I. C. Christov, Proceedings of the Royal Society A: Mathematical, Physical and Engineering Sciences **475**, 20190513 (2019).
[43] The supplementary material contains a full list of symbols, a selection of raw data for the time-dependence of flow rate and pressures; asymptotic analysis of the eigenvalue equation; and flow sensor calibration data, see [URL to be input by the publisher] .
[44] Y. Xia and G. M. Whitesides, Angewandte Chemie In-

ternational Edition **37**, 550 (1998).

[45] X. Wang and I. C. Christov, Physics of Fluids **33**, 102004 (2021).

[46] We note that the infinitely thick limit is expected when the thickness of the upper, flexible wall is roughly twice the width of the channel, which is always the case here. With the reported value [54] of ν=0.495, we have $E^* \approx 2.44E_{\mathrm{Y}}$.

[47] H. Bruus, *Theoretical Microfluidics* (Oxford University Press, 2008).

[48] A. I. Panou, K. G. Papadokostaki, P. A. Tarantili, and M. Sanopoulou, European Polymer Journal **49**, 1803 (2013).

[49] P. Tabeling, *Introduction to Microfluidics*, 1st ed. (Oxford University Press, 2010).

[50] A. Oron, S. H. Davis, and S. G. Bankoff, Reviews of modern physics **69**, 931 (1997).

[51] V. Placet and P. Delobelle, Journal of Micromechanics and Microengineering **25**, 035009 (2015).

[52] B. K. Wunderlich, U. A. Kleßinger, and A. R. Bausch, Lab Chip **10**, 1025 (2010).

[53] DLMF, "*NIST Digital Library of Mathematical Functions*," http://dlmf.nist.gov/, Release 1.1.5 of 2022-03-15, f. W. J. Olver, A. B. Olde Daalhuis, D. W. Lozier, B. I. Schneider, R. F. Boisvert, C. W. Clark, B. R. Miller, B. V. Saunders, H. S. Cohl, and M. A. McClain, eds.

[54] A. Müller, M. C. Wapler, and U. Wallrabe, Soft Matter **15**, 779 (2019).